LAWRENCE
LIVERMORE
NATIONAL
LABORATORY

LLNL-CONF-843035

Correcting Gain Drift in TES Detectors for Future X-ray Satellite Missions

S. J. Smith, M. C. Witthoeft, J. S. Adams, S. R. Bandler, S. Beaumont, J. A. Chervenak, R. S. Cumbee, M. E. Eckart, F. M. Finkbeiner, S. V. Hull, R. L. Kelley, C. A. Kilbourne, M. A. Leutenegger, F. S. Porter, K. Sakai, N. A. Wakeham, W. J. Wassell

December 7, 2022

Applied Superconductivity Conference - ASC 2022
Honolulu, HI, United States
October 23, 2022 through October 28, 2022

Disclaimer

Correcting Gain Drift in TES Detectors for Future X-ray Satellite Missions

Stephen J. Smith, Michael C. Witthoeft, Joseph S. Adams, Simon R. Bandler, Sophie Beaumont, James A. Chervenak, Renata S. Cumbee, Megan E. Eckart, Fred M. Finkbeiner, Sam V. Hull, Richard L. Kelley, Caroline A. Kilbourne, Maurice A. Leutenegger, Frederick S. Porter, Kazuhiro Sakai, Nicholas A. Wakeham and Edward J. Wassell

***Abstract*— Changes in the operating environment of transition-edge sensor (TES) microcalorimeters can cause variations in the detector gain function over time. If not corrected, this can degrade the spectral resolution, and cause systematic errors in the knowledge of the absolute energy. The non-linear nature of the TES energy scale function and the potential for multiple, simultaneous sources of drift can make effective corrections extremely challenging. Satellite instruments typically employ an on-board calibration source to provide known reference X-ray lines. This allows real-time monitoring of the detector gain stability and provides information that can be used to correct for drifts. Here we discuss progress towards demonstrating that the energy scale requirements can be met for future instruments such as Athena X-IFU. We present measurements (from ~ 1-12 keV) on ~ 200 pixels in a prototype X-IFU array. We use a non-linear drift correction algorithm that uses two fiducial calibration lines (5.4 keV and 8.0 keV) to track gain and interpolate a new, corrected gain between a set of three pre-calibrated gain functions that span the anticipated range of induced drifts. We demonstrate this algorithm is effective at correcting the full gain scale in the presence of multiple sources of environmental drift.**

***Index Terms*— Athena space telescope, imaging array, energy-scale calibration, transition-edge sensor, X-ray spectroscopy.**

I. Introduction

Transition-Edge Sensors (TESs) are high energy resolution, non-dispersive detectors, being developed for the next generation X-ray spectrometer instruments on board future space telescopes. This includes ESA's Athena mission [1] and NASA's Lynx [2] and LEM mission concepts [3]. The X-ray Integral Field Unit (X-IFU) is an instrument onboard Athena that will provide high-resolution (2.5 eV at energies up to 7 keV) spatially resolved (5") spectroscopy over the energy range 0.2–12 keV. X-IFU will have an array of over 2,000 TESs in a hexagonal configuration, covering a field-of-view of ~ 5'.

TESs measure the heat from the thermalization of an X-ray photon and are based on superconducting thin films, which are voltage biased in their superconducting-to-normal transition. The resistance change is determined by measuring the current through the TES using a superconducting quantum interference device (SQUID). Digital optimal filtering is used to convert the measured raw current pulse to a pulse-height estimate [4], which is then converted into energy units using the detector energy scale (or gain) function.

Microcalorimeters are thermal detectors and, as such, their energy scale function is sensitive to the environmental conditions. Temporal changes in parameters such as the heat-sink temperature at which the detectors are operated, the TESs local magnetic field environment, the TES bias DAC, radiative power loading and the temperature of the readout amplifiers, may result in the drift of the energy scale function over time. If left uncorrected, this can degrade the energy resolution and result in systematic errors in the absolute knowledge of the energy scale. Space telescopes employ an on-board calibration source that provides known reference X-ray lines. This provides real-time monitoring of the gain stability of the detector system and information that can be used to correct for temporal drifts in post processing. Porter et al. (2016) developed a correction algorithm used for the Soft X-ray Spectrometer (SXS) instrument on board the Hitomi mission [5]. This approach was based around tracking the temporal gain drift using a single fiducial line (for example Cu-Kα X-rays), and then interpolating a new energy scale from prior ground calibration measurements. This was shown to be effective at recovering the gain to below the 2 eV energy-scale requirement for energies up to 12 keV [5], [6]. However, TESs are significantly more non-linear than the Si thermistors used for SXS/Hitomi and the requirements for future missions such as Athena are significantly more challenging

Manuscript receipt and acceptance dates will be inserted here. S. Hull's research was supported by an appointment to the NASA Postdoctoral Program at the NASA Goddard Space Flight Center, administered by Oak Ridge Associated Universities under contract with NASA. This material is in-part based upon work supported by NASA under award number 80GSFC21M0002. Part of this work was performed under the auspices of the U.S. Department of Energy by Lawrence Livermore National Laboratory under Contract DE-AC52-07NA27344. *(Corresponding author: Stephen J. Smith.)*

S. J. Smith, J. S. Adams, S. R. Bandler, S. Beaumont, J. A. Chervenak, R. S. Cumbee, F. M. Finkbeiner, S. V. Hull, R. L. Kelley, C. A. Kilbourne, M. A. Leutenegger, F. S. Porter, K. Sakai, N. A. Wakeham, E. J. Wassell and M. C. Witthoeft are with the National Aeronautics and Space Administration, Goddard Space Flight Center, Greenbelt, MD 20771, USA. (e-mail: stephen.j.smith@nasa.gov; joseph.s.adams@nasa.gov; simon.r.bandler@nasa.gov; sophie.beaumont@nasa.gov; james.a.chervenak@nasa.gov; renata.s.cumbee@nasa.gov fred.m.finkbeiner@nasa.gov; sam.v.hull@nasa.gov; richard.l.kelley@nasa.gov; caroline.a.kilbourne@nasa.gov; maurice.a.leutenegger@nasa.gov; frederick.s.porter@nasa.gov; kazuhiro.sakai@nasa.gov; nicholas.a.wakeham@nasa.gov; edward.wassell@nasa.gov; michael.c.witthoeft@nasa.gov).

M. E. Eckart is with Lawrence Livermore National Laboratory 7000 East Avenue, Livermore, CA 94550, USA (e-mail: eckart2@llnl.gov).

Color versions of one or more of the figures in this paper are available online at http://ieeexplore.ieee.org.

Digital Object Identifier will be inserted here upon acceptance.

(< 0.4 eV for energies up to 7 keV). In this paper, we test the non-linear correction algorithm on TES pixels in a prototype Athena X-IFU array. We examine the effectiveness of the correction algorithm to various sources of environmental drifts. We test the 1-line correction method and then extend the analysis to investigate how adding a 2nd fiducial line in the correction algorithm may improve the correction over the whole bandpass. This is the proposed method for Athena X-IFU but is yet to be demonstrated on real devices.

II. Method

A. Non-linear drift correction algorithm

The energy scale is a function $E(PH)$ that relates the output of the event processor, PH (the optimally filtered pulse height in engineering units), to calibrated energy units, E. Non-linearity in TESs arises from both the voltage bias nature of the TES bias circuit and the shape of the temperature and current dependent resistive transition $R(T,I)$. The superconducting-to-normal transition is difficult to model accurately, thus an empirical approach to gain calibration is required. The energy scale is found by fitting some function (such as a polynomial) to the known positions of the X-ray calibration points as a function of PH. Variations in the detector's environment result in drifts in the energy scale over time. Not every source of drift affects the energy scale in the same way. Changes in the TES voltage bias,

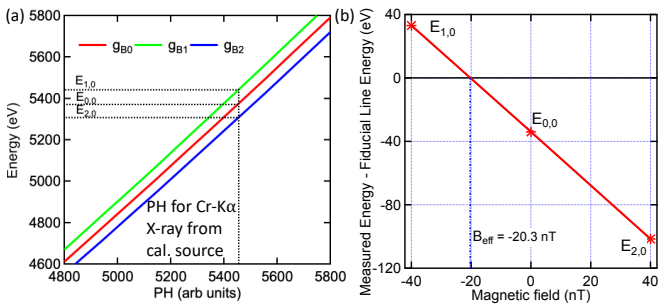

Fig. 1. Derivation of B_{eff} used to correct the energy scale using the 1-line non-linear correction. (a) The three energy scale functions g_k, measured at 3 different magnetic fields B_k = (0, −40 nT, +40 nT) are applied to the measured PH_0 from Cr-Kα X-rays from the calibration source. This gives three estimates for the photon energy $E_{k,0}$. (b) By fitting a quadratic to $(E_k - E_0)$ vs B we can find the effective magnetic field B_{eff} which satisfies $(E_{k,0} - E_0) = 0$.

dV_b, will directly affect the bias point of the TES and therefore affect its gain. Changes in the heat-sink temperature (and radiative loading), dT will have a similar impact since it directly changes the operating point of the TES but can also slightly affect other properties such as the transition shape (due to the current and magnetic field dependence of the transition). Magnetic field variations, dB, directly affect the TES transition shape via the temperature and field dependent critical current. Changes in $R(T,I)$ directly affect the pulse shape and thus the gain of the detector. Additional linear drifts, dL, may also be present due to temperature variations in the room temperature electronics. With the potential for several simultaneous sources of gain drift, an effective correction to the energy scale is particularly challenging. In orbit, a Modulated X-ray Source (MXS) [7] will be used to provide an X-ray line(s) at a known energy, E_0, (or energies) and is used to monitor the detector drift over time. We measure the $PH_0(t)$ of this fiducial line, typically by taking some time-average of a group of events to reduce the impact of statistical noise. The simplest method to correct the gain would be to apply a proportional stretch factor to the measured PH so that $E_0 = E[\alpha(t)\, PH_0(t)]$, where $\alpha(t)$ is a time-dependent factor that moves the PH of the fiducial line to the PH value expected by the gain. However, this is sufficiently accurate only when the gain function is close to linear and/or drifts are small. An improved method developed in [5] uses the non-linear shape of the energy scale function to correct for temporal drifts. During ground calibration, three energy scale functions are measured $g_k(PH)$ where $k \in (0,1,2)$. Each function is measured under a different environmental condition q_k, which forms the basis set for the correction. For Hitomi/SXS, the basis for the correction was heat-sink temperature ($q = T$, with T_0 = 50 mK, T_1 = 49 mK, T_2 = 51 mK). These were chosen to span (with significant margin) the anticipated range of induced drifts over the course of the mission lifetime. In principle, any basis can be chosen (heat-sink temperature, magnetic field, TES bias etc). In this paper, we primarily focus on magnetic field ($q_k = B_k$), since this is potentially the largest source of gain variation for Athena X-IFU. We apply all three gain functions g_k to the measured $PH_0(t)$ to find three estimates of the photon energy, $E_{k,0}(t) = g_k\big(PH_0(t)\big)$. The difference between the inferred energies $E_{k,0}(t)$ and the known energy of the fiducial line is:

$$y_k(t) = E_{k,0}(t) - E_0. \tag{1}$$

We can then construct a quadratic fit $y(B_k;t)$ to the energy difference y_k versus the parameter B_k. This allows us to compute an effective parameter, $B_{eff}(t)$, which is defined so that $y(B_{eff}) = 0$. This is essentially a calculation of the environmental parameter under which the measurement must have been taken assuming no drift in any other environmental conditions. Figure 1 shows a graphical representation of this process. The derived effective parameter, $B_{eff}(t)$, can then be used to construct an interpolated energy scale to correct photon energies as a function of time. The new energy scale, $g_{eff}(PH,t)$, is calculated using a 3-point Lagrange interpolation between the reference gain scales (see Fig. 2a)

$$g_{eff}(PH,t) = \sum_k l_k(t)\; g_k(PH) \tag{2}$$

$$l_k(t) = \prod_{m \neq k} \frac{B_{eff}(t) - B_m}{B_k - B_m} \tag{3}$$

This approach was highly effective for SXS/Hitomi at correcting large temperature offsets (rather than magnetic field offsets) and was also found to have some ability to correct for other sources of drift [5]. However, in the simulations of Cucchetti et al. [8], [9] even the non-linear approach was predicted to have limitations when compared to the stringent X-IFU requirements. This motivated the extension of the 1-line method to incorporate a second fiducial line. In the 2-line approach, we independently apply the method described above to each fiducial line to obtain effective parameters, $B_{eff,1}$ and $B_{eff,2}$. Then, using linear interpolation, we obtain $B_{eff}(E,t)$, which can be used in (3). Figure 2b shows an example of $B_{eff}(t)$ using the 2-line

correction (at Cr-Kα and Cu-Kα) for a single representative pixel exhibiting a large energy dependence to $B_{\rm eff}$. Since this method forces the energy to be correct at two reference points the broad-band errors in gain scale may be reduced. This may be particularly powerful when correcting for sources of drifts that affect the gain differently to the basis set $g_{\rm k}$.

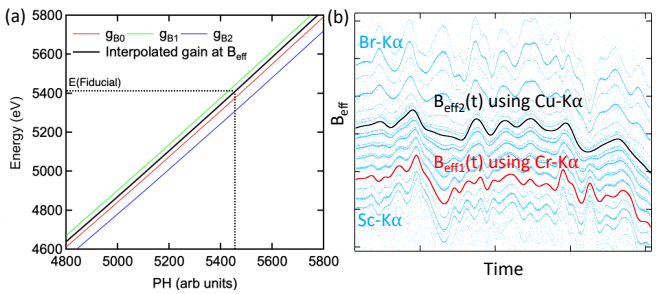

Fig. 2. (a) The corrected gain scale (black line) is derived at $B_{\rm eff}$ by interpolating the reference gain scales $g_{\rm k}$. (b) Example effective magnetic field $B_{\rm eff}(t)$ for showing X-ray lines from 4 keV (Sc-Kα) to 12 keV (Br-Kα). In this example we use 2-lines from the calibration source and now have 2 independent $B_{\rm eff}$(t) estimates (Cr-Kα - red dots, and Cu-Kα - black dots). Linear interpolation across the two estimates $B_{\rm eff,1}$ and $B_{\rm eff,2}$ results in an energy dependent $B_{\rm eff}$ (blue dots), which is used to correct the gain.

B. Detector design and experimental approach

Measurements were carried out on a prototype Athena X-IFU array consisting of 1k pixels. The devices consisted of 50 µm x 50 µm Mo/Au TESs with a transition temperature of 90 mK. Pixels were fabricated on a 250 µm pitch and used Bi/Au electroplated absorbers. Approximately 200 pixels in the array are readout using 8-column x 32-row Time Division Multiplexing (TDM). The pixels had a normal state resistance of $R_{\rm n}$ ~ 8 mΩ and are operated at 10% $R_{\rm n}$ with heat-sink temperature of 55 mK. These devices demonstrated a spectral resolution 2 eV for energies up to ~ 6 keV. Further details on the design and performance of these types of pixels and this array can be found in [10], [11]. X-rays were generated using rotating target sources (RTS) [6]. Each RTS contained up to 16 target disks (high purity metals or crystals) that could be rotated in turn into a primary X-ray beam. This generated fluorescent Kα and Kβ X-ray emission characteristic of the target material. We used an RTS that generated X-rays in air, which then passed through a Be window installed on a gate valve on the cryostat exterior (without a direct connection to the cryostat). This was used for energies above 3 keV which easily penetrate through air. A separate vacuum-RTS (V-RTS) was directly attached to a gate valve, sharing vacuum with cryostat, and was used for testing energies below 3 keV. The count-rate per pixel ranged from 0.4 to 2.0 cps/pixel, depending upon the target and type of RTS. The hold time on each target was tuned such that the total number of events measured was approximately equal for all targets during one full rotation period (~ 4 mins). Data was measured continuously over the 60 hr hold time of the Adiabatic Demagnetization Refrigerator (ADR), amounting to ~ 40M X-ray events in a single data set. Measurements were initially carried out over the 3-12 keV (K-Kα to Br-Kα) energy range using the RTS and follow-up measurements were carried out to test the lower energies from 1.3-8.6 keV (Mg-Kα to Zn-Kα) using the V-RTS. An optimal filter template was generated at 6 keV (Mn-Kα) under the nominal environmental conditions for every pixel. This set of templates was used for all the analyses.

For this array we have found that the average detector gain sensitivities at Co-Kα (6.9 keV) to magnetic field, heat sink temperature, TES bias voltage and linear amplification are $\langle dE/dB\rangle = (1.95 \pm 0.13)$ eV/nT, $\langle dE/dT\rangle = (94.2 \pm 4.3)$ meV/µK, $\langle dE/dV_b\rangle = (12.8 \pm 1.4)$ meV/ppm and $\langle dE/dL\rangle = (8.77 \pm 0.07)$ meV/ppm, respectively. Because the X-IFU will be launched warm, different static magnetic fields may be trapped in the superconducting Nb shielding when re-cooling down in space, compared to prior ground calibration. The full requirements are still being developed but the aim is to limit magnetic field variation to dB < 5 nT, which would result in maximum energy error of 10 eV at 7 keV, if uncorrected. The other anticipated environmental variations are assumed as dT < 150 µK, d$V_{\rm b}$ < 300 ppm and dL < 1000 ppm. These induce a similar magnitude of gain error to dB. We have tested using both B and T, independently, as the basis for the gain scale correction with similar findings. However, here we present results using B as the basis. Since the currently assumed requirement on dB enforces extremely challenging magnetic shielding requirements on the instrument, it is important to probe the maximum dB range over which we can correct the gain, in case the shielding requirements cannot be satisfied. We choose our $g_{\rm k}$ curves at $B_{\rm k}$ = (0 nT, -40 nT, +40 nT). This is sufficient to bound the induced gain errors from these various sources of environmental drift. We tested the effectiveness of both the 1- and 2-line corrections by remeasuring the energy scale at various fixed offset values of dB, dT, d$V_{\rm b}$ (to much larger values than the X-IFU requirements.) The fiducial lines used in the corrections were Cr-Kα (5.4 keV) and Cu-Kα (8 keV), the other RTS lines are used to evaluate the gain correction residuals.

III. Results and Analysis

Figure 3a shows a representative energy scale, $g_{0,}$ (measured over 3-12 keV) for one pixel. The energy scales were derived from measured events and therefore contain errors arising from event statistics, uncertainties in the assumed literature line profiles used to fit the measured complexes, and errors in the ability of the polynomial fitting function to accurately recreate the true gain shape. Higher order polynomial fits can in principle be used to reduce the gain error at the calibration lines (forcing the fit to go through the data points) but this may introduce interpolation errors away from those calibration points (and assumes there is no error in the assumed line profile positions). The 8$^{\rm th}$ order fit was chosen as a reasonable compromise. For X-IFU the objective is to fit an individual energy scale at the level of < 0.1 eV. This is challenging and an active area of research. In this study, we were not trying to directly demonstrate the ability to meet the absolute energy scale requirements but trying to demonstrate how well we can correct for systematic offsets/drifts due to changes in the environment for a given set of reference gain scales.

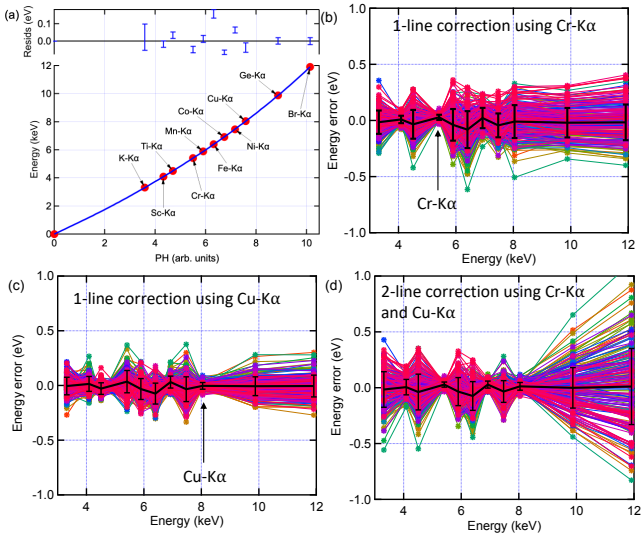

Fig. 3. (a) Example energy scale measured over the energy range 3.3-12 keV for a single representative pixel, fitting with an 8th order polynomial. Also shown are the 1-line gain correction residuals using fiducial X-rays from (b) Cr-Kα and (c) Cu-Kα. (d) Residuals using the 2-line correction (Cr-Kα and Cu-Kα). The black line shows the mean of all pixels with 1-sigma error bars.

We first applied the 1- and 2-line algorithms to the data set used to construct the B_0 energy scale. This provided an estimate of the baseline correction residuals (due to statistics and underlying errors in the gain scale fitting) in the presence of no additional environmental offsets. Figure 3b-d shows the gain residuals using the 1-line and 2-line corrections. The statistical fit errors associated with the position of the line complexes are typically ≤ 0.06 eV, thus the errors in the energy estimation are predominately associated with the residual errors in the underlying gain-scales (similar results were achieved testing at B_1 and B_2). Since the non-linear correction works by forcing the errors at the fiducial line(s) to zero, any errors in the reference gain scales at those fiducial lines must therefore be re-distributed

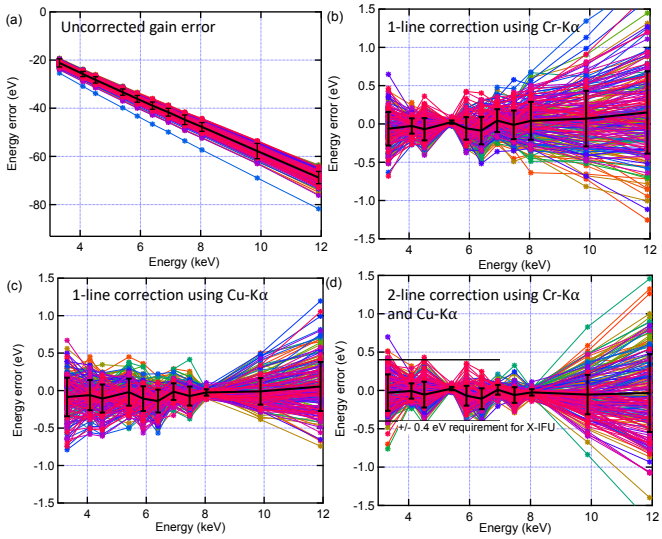

Fig. 4. (a) Uncorrected gain residuals for 200 pixels with dB = −20 nT, measured over the energy range 3.3-12 keV. Also shown are the 1-line gain correction residuals using fiducial X-rays from (b) Cr-Kα, (c) Cu-Kα and (d) the 2-line residuals using both Cr-Kα and Cu-Kα. The black lines show the mean of all pixels with 1-sigma error bars.

across the energy band in the derived gain scale. For the 1-line algorithm, the errors are mostly distributed uniformly across the whole energy range because $B_{\rm eff}$ has no energy dependence. However, with the 2-line algorithm, $B_{\rm eff}$ depends linearly on energy and the error on the slope of $B_{\rm eff}$ causes energy errors to worsen with increasing energy (> 8 keV). In both cases, since the errors are primarily due to the underlying residuals in the reference gain scales, better gain scales will directly lead to better performance of these algorithms.

We next introduced an offset, dB = −20 nT, at the midpoint between the calibration curves g_0 and g_2. Since this is the farthest point from the calibration curves (and much larger than the ±5 nT requirement), it corresponds to the most challenging case that must be corrected. Figure 4 shows (a) the uncorrected gain errors, (b) the correction residuals using a 1-line correction at Cr-Kα, (c) the same for Cu-Kα, and (d) the 2-line correction using both Cr-Kα and Cu-Kα. The 1-line corrections were both effective at recovering the energy scale in the presence of a large dB. We find that the average $B_{\rm eff}$ across all pixels are almost identical when using either the Cr-Kα or Cu-Kα fiducial, $B_{\rm eff,1}$ = (−19.70±0.31) nT and $B_{\rm eff,2}$ = (−19.67±0.29) nT, and closely matches the applied field of −20 nT. This is consistent

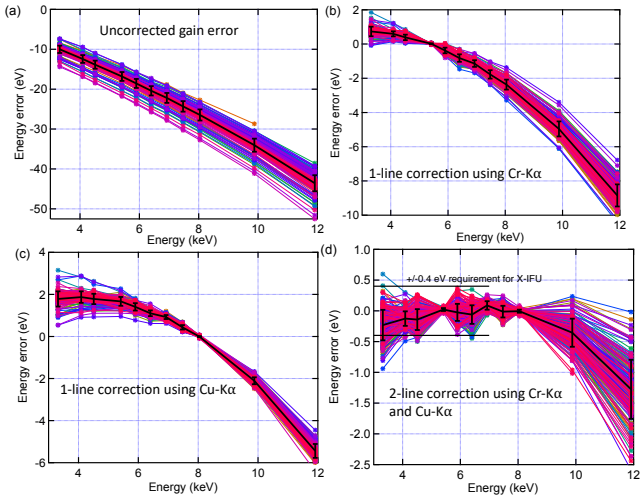

Fig. 5. (a) Uncorrected gain residuals for 200 pixels with dT = 250 μK, measured over the energy range 3.3-12 keV. Also shown are the 1-line gain correction residuals using fiducial X-rays from (b) Cr-Kα, (c) Cu-Kα and (d) the 2-line residuals using both Cr-Kα and Cu-Kα. The black lines show the mean of all pixels with 1-sigma error bars.

with fact that the mean residual of all pixels (thick black line) is close to zero across the measured energy range. The variance amongst pixels was slightly worse than in the baseline case (Fig. 3) and was likely due to the combined effects of errors in the underlying gain scales and interpolation errors across the reference gains. That the 2-line residuals are better at energies < 10 keV shows the importance of including energy dependence into the estimated parameter. Overall, this demonstrated that the 1- and 2-line algorithms are highly effective at re-constructing an accurate gain scale at an arbitrary B. Since this represents the most challenging case to correct for, this result suggests the nominal < 0.4 eV requirement for X-IFU should be satisfied over the full g_k calibration space (±40 nT). Similar results were obtained with V-RTS at energies down to 1.3 keV (Mg-Kα).

We also used the non-linear algorithms (in the B-field basis set) to correct for other sources of drift that affect the gain differently to dB. Figure 5 shows an example for dT = 250 μK which gave a factor of ~ 2 lower uncorrected gain errors compared to the dB = –20 nT case. The 1-line corrections forced the fiducials to the correct position at the reference line, however there was a clear systematic bias across the bandpass. This is because gain changes due to dT are quite different to gain changes from dB. Thus, forcing the gain to be correct at the fiducials gives substantial errors elsewhere. It also follows that, unlike correcting for dB, the calculated $B_{\rm eff}$ should have significant energy dependence. Averaged over all pixels we found $B_{\rm eff,1}$ = (9.91±0.63) nT at Cr-Kα, and $B_{\rm eff,2}$ = (10.88±0.63) nT at Cu-Kα, a difference of 0.9 nT. The $B_{\rm eff}(E)$ versus time for a representative pixel is shown in Fig. 2b. These $B_{\rm eff}$ values have no physical relation to temperature, they are simply the mapping of the dT into an equivalent dB. The 2-line correction offers significant advantages when correcting for drifts that are of different origin as the basis set (Fig. 5d). By forcing the energy to be correct at both fiducial lines, and linearly interpolating $B_{\rm eff}$ across the full band-pass, we significantly reduced (but not entirely eliminated) the residual bias in the correction.

Additional measurements were carried out with dB and dT offsets over the range dT = 125 μK to 750 μK and dB = ±20 nT. This included measurements using the V-RTS to extend the analysis down to 1.25 keV (Mg-Kα). The results are summarized in Fig. 6 for the 2-line correction only. Here we only show the mean of all pixels for each measurement. We have subtracted the baseline mean measured at (dT, dB) = (0 μK, 0 nT) (Fig. 3c) to remove any systematics residuals due to the underlying gain scales. This leaves only the residual error from the non-linear correction itself. Since we are constraining the residuals to zero at the fiducial lines and at zero energy, it follows that the underlying shape of the residuals should be

$$\delta E = E\,(E - E_{\rm CrK\alpha})(E - E_{\rm CuK\alpha})\,p(E), \qquad (4)$$

where $p(E)$ is an unknown function depending on the shape of the actual gain. We fit the $\boldsymbol{\delta}E(E)$ curves in Fig. 6 curves using a 5th order polynomial as a guide. We note several key findings:

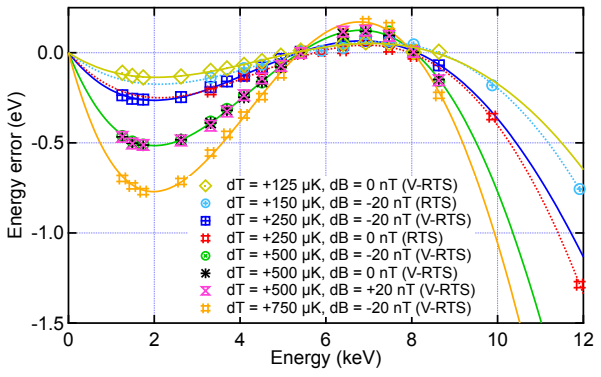

Fig. 6. Mean gain correction residuals $\boldsymbol{\delta}E(E)$ across all pixels for dT and dB offsets as indicated on the legend. Both high energy RTS (3.3-12 keV) and low energy V-RTS (1.3-8.6 keV) measurements are included. The lines are 5th order polynomial fits to guide the eye. The magnitude of the gain correction residuals only depends on dT and scale approximately linearly with dT. The maximum drifts that X-IFU will be subject to is d$T_{\rm b}$ ~ ±150 μK and dB = ±5 nT.

1) The residuals are consistent where the energy range overlaps between high and low energy RTS datasets.
2) The gain residuals only depend on dT (dB offsets can be corrected with zero residual bias). This is illustrated by data sets taken at dT = 500 μK, combined with dB = 0, ± 20 nT). These 3 cases have very different uncorrected gain errors. However, after the non-linear correction, the residuals are essentially identical.
3) The magnitude of the gain residuals scales approximately linearly with dT.
4) The pixel-to-pixel variance around the mean tends to zero at the reference points (following (4)), increasing away from those points and as the mean energy error increases.

The algorithm is effective over a very large parameter space. At the notional X-IFU limit of dT ~ ±150 μK, the maximum bias at energies up to 7 keV is just 0.17 eV. The examples at (dT, dB) = (500 μK, –20 nT) and (dT, dB) = (750 μK, –20 nT) both result in uncorrected gain errors that are outside the bounds of the $g_{\rm k}$ calibration phase-space (> 100 eV at 7 keV). In this scenario the non-linear correction extrapolates beyond the measured phase-space but still corrects the gain very effectively. This suggests that more widely spaced $g_{\rm k}$ curves could be used to correct for even larger dB in future measurements.

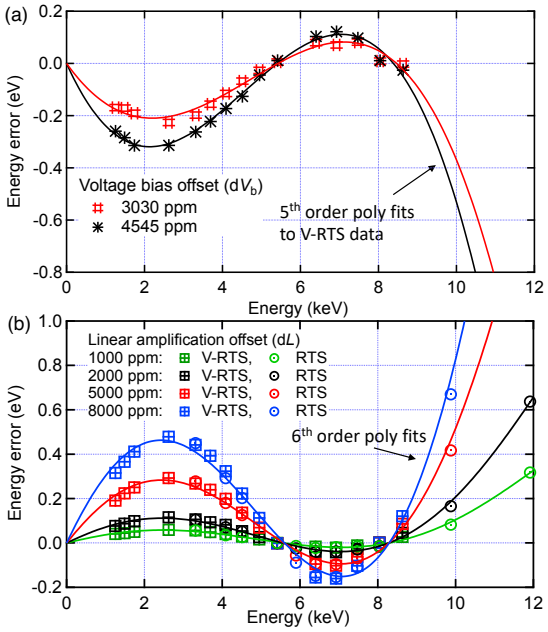

Fig. 7. (a) Mean gain correction residuals $\boldsymbol{\delta}E(E)$ across all pixels for offsets in (a) d$V_{\rm b}$ and (b) dL. For all curves (dT, dB) = (0 μK, 0 nT). The maximum drift that X-IFU will be subject to is d$V_{\rm b}$ = ±300 ppm and dL = ±1000 ppm.

Figure 7a shows a similar analysis for various TES voltage bias offsets, d$V_{\rm b}$, and Fig. 7b for linear amplification offsets, dL (extending well beyond the X-IFU requirements). Since dL is a linear gain factor, we used the same data measured at (dT, dB) = (0 μK, 0 nT) and applied a stretch factor (1000, 2000, 5000, and 8000 ppm) to the $PH(t)$ values, before applying the 2-line correction. The 2-line correction was again highly effective in correcting these large offsets whereas the 1-line method leaves

significant residuals. The energy dependence of the residuals is qualitatively similar to those shown in Fig. 6 for dT offsets. At the X-IFU environment requirements the maximum bias at energies < 7 keV is: ~ 0.02 eV for dV_b = 300 ppm, and ~ 0.07 eV for dL = 1000 ppm. Substantially less than the 0.4 eV overall requirement.

IV. CONCLUSION

We have tested a non-linear drift correction algorithm on TES detectors developed for X-IFU. By choosing B as the basis set for the non-linear correction, and using two fiducial lines to track offsets, we have demonstrated we can correct dB over the range ±40 nT (x8 larger than the X-IFU requirement.) The power of the two-line correction is that it can also suppress various other sources of gain variation, that affect the energy scale quite differently to B, leaving low residual bias in the energy scale. These results are extremely encouraging for ultimately being able to meet the stringent X-IFU energy scale knowledge requirement of < 0.4 eV, although some challenges remain.

One challenge is the ability of measure a single energy scale to sufficient absolute accuracy. The ability to fit the calibration points when constructing the energy scale coupled with uncertainties in the line shapes of the fluoresced targets from the RTS result in absolute energy errors. This is currently a limiting factor. In future work we will explore more optimal fitting functions as well as the use of an Electron Beam Ion Trap (EBIT), which can generate narrow X-ray lines from highly charged (H-like and He-like) ions that have well known energies [12].

In the final flight instrument, there will also be noise due to the available statistics from the MXS used to track the gain over time. To limit these effects, calibration photons from groups of ~10 pixels must be added together before constructing the $PH_0(t)$ drift correction. The impact of statistics and drift correcting based on multiple pixels needs to be explored in future work.

In parallel work, we have now demonstrated pixels with ~ 8x lower gain sensitivity to magnetic field compared to the pixels we report here [13]. For these new pixels, energy offsets from dB are much smaller than from dT. This may make it more favorable to use temperature as the correction basis, enabling better overall gain correction of both dB and dT.

Finally, we will explore incorporating additional information into the drift correction algorithm, such as the baseline level of the detector (which also contains information about the detector drift) [8], [9], and house-keeping information from the instrument (such as thermometry).

ACKNOWLEDGMENT

We would like to thank members of the Athena X-IFU performance working group (P. Peille, R. den Hartog, B. Jackson, E. Cucchetti, C. Kirsch, J. Wilms, W.B. Doriese and M. Durkin) for many useful discussions and inputs in the preparation of this work. Part of this work was performed under the auspices of the U.S. Department of Energy by Lawrence Livermore National Laboratory under Contract DE-AC52-07NA27344.

REFERENCES

[1] D. Barret *et al.*, "The Athena Xray Integral Field Unit (X-IFU): a consolidated design for the system requirement review of the preliminary definition phase", *Exp Astron* (2023). https://doi.org/10.1007/s10686-022-09880-7

[2] J. A. Gaskin *et al.*, "Lynx X-Ray Observatory: an overview," *J. Astron. Telesc. Instrum. Syst.* 5(2) 021001 (29 May 2019) https://doi.org/10.1117/1.JATIS.5.2.021001

[3] R. Kraft *et al.*, "Line Emission Mapper (LEM): Probing the physics of the cosmic ecosystem", arXiv white paper 2022. https://doi.org/10.48550/arXiv.2211.09827

[4] J. W. Fowler, B. K. Alpert, W. B. Doriese, Y. -I. Joe, G. C. O'Neil, J. N. Ullom, D. S. Swetz, "The Practice of Pulse Processing," *J. Low Temp. Phys.*, vol. 184, 2016, pp.374–381. https://doi.org/10.1007/s10909-015-1380-0.

[5] F. S. Porter *et al.,* "Temporal Gain Correction for X-ray Calorimeter Spectrometers," *J. Low Temp. Phys.* vol. 184, pp. 498–504 (2016). https://doi.org/10.1007/s10909-016-1503-2

[6] M. E. Eckart *et al.*, "Ground calibration of the Astro-H (Hitomi) soft x-ray spectrometer," *J. Astron. Telesc. Instrum. Syst.* 4(2) 021406 (13 April 2018) https://doi.org/10.1117/1.JATIS.4.2.021406

[7] C. P. de Vries *et al.*, "Filters and calibration sources for the soft x-ray spectrometer (SXS) instrument on ASTRO-H," in *Proc. SPIE*, 773213 (2010). https://doi.org/10.1117/12.855880

[8] E. Cucchetti, M. E. Eckart, P. Peille, F. S. Porter, F. Pajot and E. Pointecouteau, "Multi-parameter Nonlinear Gain Correction of X-ray Transition Edge Sensors for the X-ray Integral Field Unit", *J. Low Temp. Phys.* vol. 193, pp. 931–939 (2018). https://doi.org/10.1007/s10909-018-1912-5

[9] E. Cucchetti, M. E. Eckart, P. Peille, C. de Vries, F. Pajot, E. Pointecouteau, M. Leutenegger, C. A. Kilbourne and F. S. Porter, "Energy scale calibration and drift correction of the X-IFU," *Proc. SPIE 10699, Space Telescopes and Instrumentation 2018: Ultraviolet to Gamma Ray*, 106994M (6 July 2018); https://doi.org/10.1117/12.2312170

[10] A. R. Miniussi *et al.*, "Performance of an X-ray Microcalorimeter with a 240μm Absorber and a 50μm TES Bilayer," *J. Low Temp. Phys*., vol. 193, 2018, pp. 337-343.

[11] S. J. Smith *et al.*, "Performance of a Broad-Band, High-Resolution, Transition-Edge Sensor Spectrometer for X-ray Astrophysics," *IEEE Trans. Appl. Supercond.*, vol. 31, no. 5, pp. 1-6, Aug. 2021, Art no. 2100806, doi: 10.1109/TASC.2021.3061918.

[12] G. V. Brown *et al.*, "A brief overview of the fusion and astrophysics data and diagnostic calibration facility," in *Proc. SPIE 7732, Space Telescopes Instrum. Ultraviolet Gamma Ray*, Jul. 29, 2010, Art. no. 77324Q, [Online]. Available: https://doi.org/10.1117/12.857555.

[13] N. A. Wakeham *et al.*, "Refinement of Transition-Edge Sensor Dimensions for the X-ray Integral Field Unit on ATHENA", in *IEEE Trans. Appl. Supercond.,* 2023. doi: 10.1109/TASC.2023.3253067.